Geomechanics and Engineering, *Vol. 21, No. 5 (2020) 423-432*
DOI: https://doi.org/10.12989/gae.2020.21.5.423

Hydraulic conductivity of cemented sand from experiments and 3D Image based numerical analysis

Sathya Subramanian[1a], Yi Zhang[1a], Ganapathiraman Vinoth[2a], Juhyuk Moon[3b] and Taeseo Ku*[1]

[1]*Department of Civil and Environmental Engineering, National University of Singapore, 1 Engineering Drive 2, 117576 Singapore*
[2]*Department of Civil Engineering, The University of British Columbia, 6250 Applied Science Ln #2002, Vancouver, BC V6T 1Z4, Canada*
[3]*Department of Civil and Environmental Engineering, Seoul National University, Kwanak-gu Kwanak-ro 1, 35-412, Seoul 08826, Korea*

(Received November 22, 2019, Revised February 22, 2020, Accepted April 14, 2020)

Abstract. Hydraulic conductivity is one of the engineering properties of soil. This study focusses on the influence of cement content on the hydraulic conductivity of cemented sand, which is investigated based on the results from numerical analysis and laboratory testing. For numerical analysis the cemented samples were scanned using X-ray Computed Tomography (CT) while laboratory testing was carried out using a triaxial setup. Numerical analysis enables us to simulate flow through the sample and provides insight to the microstructure. It quantifies the pore volume, proportion of interconnected voids and pore size distribution in both cemented and uncemented samples, which could be computed only through empirical equations in case of laboratory testing. With reduction in global voids, the interconnecting voids within the samples also reduce with cement content. Gamma cumulative distribution function is used to predict the percentage of voids lesser than a given pore volume. Finally, the results obtained from both numerical analysis and laboratory testing are compared.

Keywords: lifecycle performance; stochastic deterioration modelling; structural reliability; reinforcement corrosion; residual strength

1. Introduction

Chemical stabilization, by deep cement mixing or jet grouting is one of the common methods to improve natural soil. In general, chemical stabilization of loose sand improves its strength and liquefaction resistance, prevents seepage and reduces compressibility. Ordinary Portland Cement (OPC) is widely used in soil stabilization and extensive research has been carried out to examine its properties as a cementing agent (Clough *et al.* 1981, Schnaid *et al.* 2001). While mechanical properties such as strength, stiffness, and compressibility have been extensively studied for OPC treated sand (Acar and El-Tahir 1986, Saxena *et al.* 1988, Fernandez and Santamarina 2001, Consoli *et al.* 2007, Wang and Leung 2008, Ajorloo *et al.* 2012, Subramanian *et al.* 2018, 2019, Khan *et al.* 2019, Lee *et al.* 2019, Moon *et al.* 2019, Wei and Ku 2020), only limited literature is available on studying its hydraulic conductivity owing to experimental difficulties to obtain accurate results. The ground water fluctuations can indeed affect the load carrying performance of foundations (Park *et al.* 2019). For instance, the conventional permeameter used in laboratory testing has rigid confinement which allows the water to flow along the interface between confinement and sample, thereby often resulting in erroneous permeability values (Carpenter and Stephenson 1986).

Although the use of flexible membrane in a triaxial setup minimizes the flow through the interface because of the confining stress, there are several factors such as hydraulic gradient, degree of saturation, duration of testing and aspect ratio that affect the results of permeability of a sample tested in a triaxial chamber.

Among these factors, hydraulic conductivity is more sensitive to the variation in hydraulic gradient. A number of studies have reported the influence of hydraulic gradient on the permeability of clayey soil. Dunn and Mitchell (1984) reported a decrease in permeability by a factor of 2.5 when the hydraulic gradient was increased from 20 to 200 for silty clay. Similar reduction in coefficient of permeability with increase in hydraulic gradient in a triaxial setup was observed by several authors (Edil and Erickson 1985, Carpenter and Stephenson 1986, Fox 1996). The reduction in hydraulic conductivity with increasing hydraulic gradient is attributed to the use of a back-pressure difference between top and bottom of the sample creates a non-uniform effective stress distribution across the sample. The larger effective stress at the outflow end can close the cracks and fissure present in the soil. Also, the non-uniform effective stress could cause seepage induced consolidation in the soil (Daniel 1994). Larger hydraulic gradient could also cause migration of fine soil particle or induce piping, which could result in unreliable estimation of coefficient of permeability (Olson and Daniel 1981, Leonards *et al.* 1991, Fox 1996). Besides these factors, the range of permeability values reported in the literature vary over a wide range compared to other mechanical properties such as undrained shear strength, friction and compression index.

*Corresponding author, Assistant Professor
E-mail: ceekt@nus.edu.sg
[a]Ph.D. Student
[b]Associate Professor

ISSN: 2005-307X (Print), 2092-6219 (Online)

Literature available on hydraulic conductivity of artificial cemented sand is scarce (Cardoso 2017) because the primary focus has been on characterizing the strength and stiffness behavior of cemented sand. Cementation, through natural or artificial process, even in small amount could alter the soil characteristics significantly. Natural cementation occurs through the precipitation of calcite between sand particles. Simulating natural cementation in laboratory can be carried out through microbially induced carbonate precipitation (MICP). Studies have shown that MICP reduces the permeability of the soil and affects the mechanical behavior of the soil (Ferris *et al.* 1996, DeJong *et al.* 2006, 2010, Al Qabany and Soga 2013, Sidik *et al.* 2014, Choi *et al.* 2019, Hang *et al.* 2019). Artificial cementation is carried out through either deep cement mixing or jet grouting. Such cemented soil shows higher strength, lesser compressibility, and improved liquefaction resistance. Artificially cemented sand has been mostly used for ground improvement or land reclamation, where the main concerns are the strength and stiffness. However, artificially cemented sands have also been used to prevent slope failure as well as hydraulic failure of excavation base. Therefore, the knowledge of the microstructure (e.g., interconnecting porosity and the size of voids inside cemented sands) and hydraulic conductivity of cemented sand is strongly required for designing appropriate hydraulic barrier.

Measuring permeability in a triaxial setup, albeit expedient, is often bound to give non-representative results due to aforementioned reasons. Instead, X-ray Computed Tomography (CT) has been utilized to examine the microstructure of natural geomaterials without cementation and then hydraulic conductivity is computed through numerical analysis (Petrovic *et al.* 1982, Hainsworth and Aylmore 1983, Crestana *et al.* 1985, Heeraman *et al.* 1997, Young *et al.* 2001, Pierret *et al.* 2002, Rogasik *et al.* 2003, Nunan *et al.* 2006). X-ray CT is a non-destructive technique that allows X-rays to pass through the material at different angles and measure the attenuation using the detector. The fundamental principles of X-ray CT are described in detail elsewhere (Ketcham and Carlson 2001). The key advantage of using X-ray CT is that it helps better understand the pore connectivity in the material and assists in visualizing real-time water movement in different soil types. Researchers often use dyes to track the water movement through the soil, which can be visualized only after destroying the sample (Mooney 2002). Also, destructive microstructure analysis using Scanning Electron Microscope (SEM) or Mercury Induced Intrusion Porosimetry (MIP) requires pre-processing of samples, which may lead to disturbance and/or change the microstructure of soil. The effect of microstructure on permeability of saturated soft clay was studied by Chen *et al.* (2019).

X-ray CT based approach would become an ideal alternative to permeability testing using conventional methods. For instance, X-ray CT has been used in geotechnical engineering to obtain the bulk density of samples, to understand pore distribution in clay and rocks (Ketcham and Carlson 2001, Mooney 2002) and to compute permeability of backfill materials (Sarkar and Siddiqua 2016). The resolution of the X-ray CT images obtained is one of the important factors that affects the estimated pore size and in turn the estimated permeability of the samples. Peng *et al.* (2014) found that low resolution images may not capture the smaller pores in Berea sandstone, but, that resulted only in a slight inaccuracy in the measurement of hydraulic conductivity.

Literatures reported on X-ray CT technique so far have focused on uncemented clayey soils and rocks (Kozaki *et al.* 2001, Kawaragi *et al.* 2009, Peng *et al.* 2014, Sarkar and Siddiqua 2016). There is no outstanding literature reported on the use of X-ray CT for computing the hydraulic conductivity of cemented sand. In laboratory testing, porosity and tortuosity of cemented samples could only be obtained through empirical relationships, but with the use of non-destructive technique such as X-Ray CT, visualization of void arrangement and tortuosity of cemented samples is possible. Thus, X-Ray CT gives great insights and surprising observations with low experimental effort to understand structure of the soil (Viggiani *et al.* 2015). This study aims to investigate the feasibility of evaluating the hydraulic conductivity of cemented sand from the X-ray CT based 3D structure. The influence of cement content on global porosity and interconnecting porosity in cemented sand is further analyzed from the image using numerical analysis. Finally, the hydraulic conductivity values obtained from numerical simulation on the 3D structure are compared against those from laboratory testing.

2. Experimental work

2.1 Materials

The uniformly graded sand used in this study is obtained from River sand Pvt. Ltd. Fig. 1 shows the particle size distribution curve obtained from sieve analysis and other index properties.

The soil is classified as Sand 'Sa' according to BS EN ISO 14688-1:2002+A1:2013. The cementing agent used is Ordinary Portland Cement Type 1. The composition of OPC obtained from X-ray diffraction analysis is shown in Fig. 2.

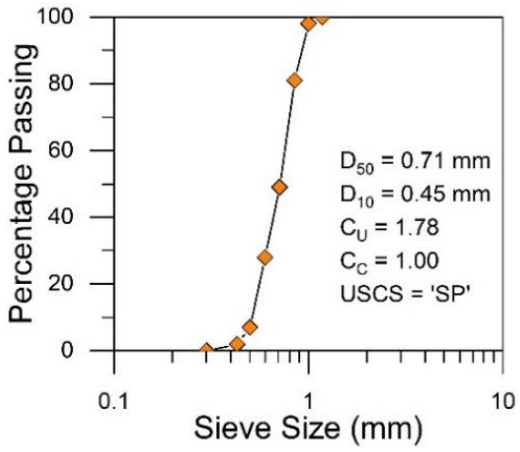

Fig. 1 Grain size distribution of sand (D_{50} – Median size of particles, D_{10} – Effective size of particles, C_u – Uniformity coefficient, C_c – Coefficient of curvature)

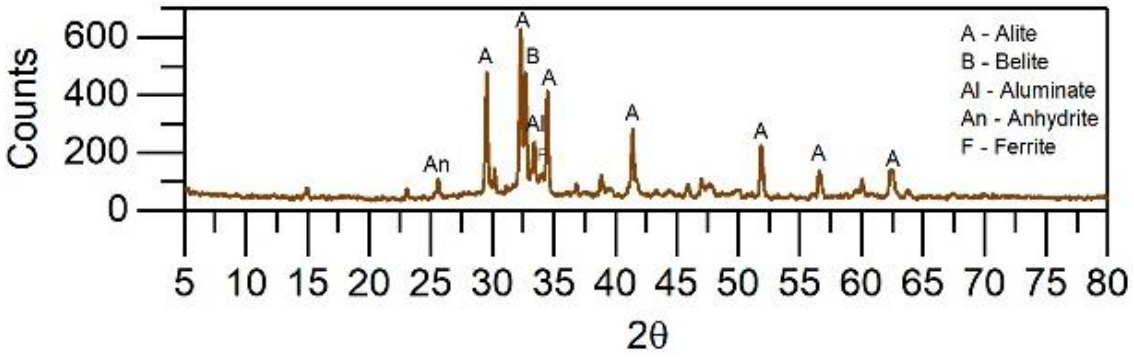

Fig. 2 X-Ray diffraction analysis on OPC Type 1

2.2 Sample preparation

The cement content used in this study is defined as a ratio of mass of cement to that of dry sand, while the water content is the ratio of mass of water to solids (includes both sand and cement). The desired quantity of dry sand with roughly half of the required amount of water is mixed in a Hobart mixer for five minutes. Thereafter, the required quantity of cement is added to the moist sand and then the remaining water is further added to the soil-cement mixture. Each stage of mixing is carried out for five minutes.

Samples for experimental permeability testing are prepared in PVC moulds of 38 mm internal diameter and 76 mm long, while samples for image analysis are prepared in PVC moulds of 35 mm internal diameter and 70 mm long (only core of sample considered for numerical analysis). The sample is prepared in three layers using undercompaction technique (Ladd 1978). Undercompaction technique involves applying lesser compaction effort for the bottom layer and increasing the compaction effort for the top layers. The use of same compaction effort for all the three layers would result in bottom layer having higher density than the top layer, as the energy from the top layer would transfer to the bottom layers while compacting. With undercompaction technique it is possible to obtain same density for all the three layers. Identical process is followed to prepare samples of diameter and length 50 mm and 100 mm respectively, for unconfined compressive strength (UCS) test.

2.3 Methodology

The main experimental program involves measurement of permeability using a standard triaxial test equipment. The schematic diagram of the experimental setup is shown in Fig. 3.

The base pedestal is 38 mm in diameter with pore pressure and bottom back pressure lines connected to it. Both top and bottom back pressures can be controlled manually. The volume change indicator used is connected to the top back pressure line. It is ensured that the sample is completely saturated (B=0.98) due to the use of a single volume change indicator as stated in BS 1377-6: 1990. For each sample, permeability value is calculated for three different confining stresses (50kPa, 100 kPa and 150 kPa). For each confining stress, rate of flow is measured with four

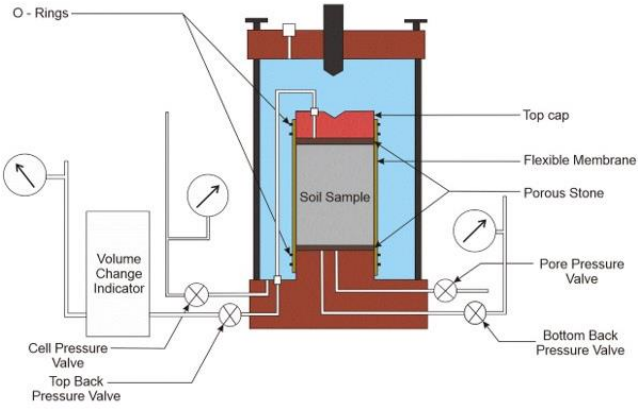

Fig. 3 Triaxial setup used for measuring permeability (modified from BS 1377-6:1990)

distinct pressure differences between top and bottom back pressures (10, 20, 30 and 40 kPa). Cemented sand samples of cement contents 3%, 5% and 7%, which corresponds to water to cement ratios of 3.43, 2.1 and 1.53 respectively, cured for 28 days under water, are used to measure permeability and unconfined compressive strength in laboratory. The post cured bulk density of 3%, 5% and 7% samples were 1.91, 1.92 and 1.93 g/cc, respectively. Also, the post-curing moisture content after 28 days for 3%, 5% and 7% samples were 20.7%, 19.2% and 18%, respectively.

An image processing software package, Avizo, is used to compute the physical properties of the materials through numerical simulation on the reconstructed 3D image of the sample. A module of XLab Hydro Extension is utilized for the permeability simulation and theoretical background is introduced in the next section. Pure sand and cemented sand samples with 1%, 3%, 5% and 7% cement content, cured for 28 days, are used for X-ray CT. Both hydraulic conductivity and unconfined compressive strength (UCS) could not be measured in the laboratory for samples of pure sand and 1% cement content as it was very difficult to extract and to mount on the triaxial or UCS test setup without disturbance.

3. Image analysis

3.1 Pre-processing and segmentation

Samples of 35 mm diameter and 70 mm length were

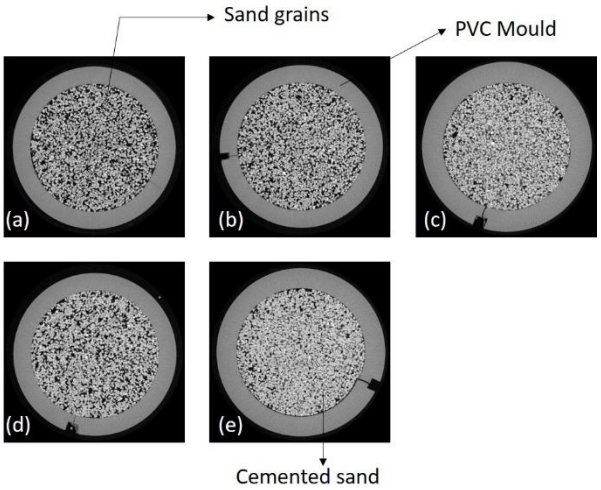

Fig. 4 1000th scanned 2D slice of (a) pure sand, (b) 1% cemented sand, (c) 3% cemented sand, (d) 5% cemented sand and (e) 7% cemented sand

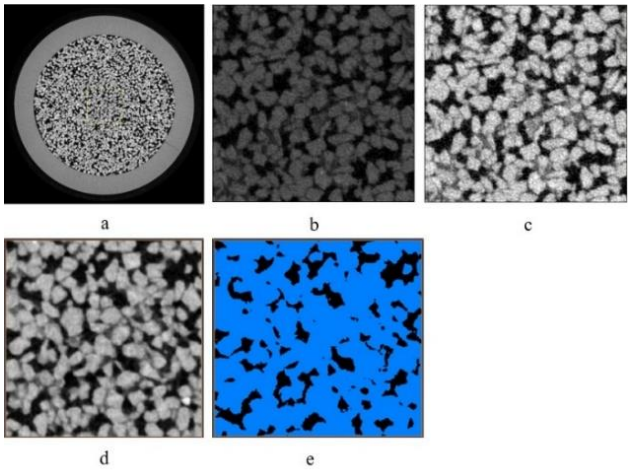

Fig. 5 Pre-processing of scanned images (a) original image, (b) cropped image, (c) brightness and contrast of cropped image adjusted, (d) de-noised images and (e) binary images (solids in blue and pore in black colour)

scanned with the PVC mould into 2240 slices of 2D images using X-ray CT. Each slice of these 2D images has an area of 2240 pixels by 2240 pixels (22 μm/ pixel). The thickness of each slice and the resolution of the pixel was chosen based on the capabilities of the X-Ray CT machine. Fig. 4 shows the 2D image of the 1000th slice of the scanned samples.

The size of volume of interest (VOI) should also be large enough to eliminate the introduction of errors due to the finite size. It has been suggested in previous literature that the minimum VOI should be at least 100 μm^3, or 3 to 5 times larger than the size of the largest distinct feature of the sample for hardened OPC pastes, to eliminate finite size error (Uchikawa 1989, Garboczi and Bentz 2001, Provis *et al.* 2012). So, in this study, 400 $voxels^3$ (around 6.84 x 10^{11} μm^3) was selected for each sample, which satisfies the size requirement in image analysis. Hence, the scanned images were cropped to 400 pixels by 400 pixels in the middle of the sample (Fig. 5(a) and 5(b)), to reduce the computation time, after which brightness of the image was adjusted for better visualization as shown in Fig. 5(c).

Then, the noise in the X-ray CT image was removed using a median filter (Fig. 5(d)). Segmentation involves converting the greyscale image to a binary image. First stage of segmentation involves classifying individual voxels with a common grey scale value named as threshold value. The thresholding value in the segmented images is ordered in terms of attenuation density where densest part (sand grain) is represented by brighter voxels and the least dense portion (pores) is represented by darker voxels as shown in Fig. 5(e). An identical thresholding value of 45/256, determined by probability distribution of attenuation density in two phase system, was selected to segment pores in all samples. Eventually, these segmented images were used to reconstruct the solid parts and compute the porosity and permeability of cemented sand.

3.2 Hydraulic conductivity simulation

On the constructed 3D structure, the absolute permeability of the samples is numerically calculated. Absolute permeability is the ability of a porous material to transmit a single-phase fluid, by hermetically closing the four sides of the samples, while imposing a pressure difference along two opposite faces to guide the water flow in one direction of the segmented microstructure image. Permeability of the sample in macro scale is computed using Darcy's law as shown in Eq. (1).

$$\frac{Q}{S} = -\frac{k}{\mu}\frac{\Delta P}{L} \tag{1}$$

where Q is the global flow rate through the sample ($m^3 \cdot s^{-1}$), S is the cross section of the sample through which fluid passes (m^2), k is the absolute permeability of the sample (m^2), μ is the dynamic viscosity of the fluid flowing through the sample (Pa·s), ΔP is the pressure difference at which fluid flows through the sample (Pa) and L is the length of the sample in flow direction (m).

Stokes' equation is solved, as shown in Eq. (2), to numerically calculate the absolute permeability of the sample. The equation is the simplification of Navier-Stokes equations, assuming an incompressible and Newtonian fluid having a laminar and steady state flow.

$$\vec{\nabla} \cdot \vec{V} = 0 \tag{2}$$

where $\vec{\nabla}.$ is the divergence operator, $\vec{\nabla}$ is the gradient operator, $\vec{V}$ and P are the velocity and pressure of the fluid in fluid phase of the material and ∇^2 is the Laplacian operator. Narsilio *et al.* (2009) verified the theoretical link between Darcy's Law (macroscale) and Stokes equations (microscale). The boundary conditions used for computing permeability are (a) no-slip condition at the solid-fluid interface, (b) fluid being able to spread freely on the face of the sample and (c) flow being isolated within the system. Once Stokes' equation is solved, Darcy's Law is applied to estimate the coefficient of permeability.

4. Results and discussion

4.1 Laboratory testing

One of the important properties that are generally used to characterize cemented soils is their unconfined compressive strength (Sariosseiri and Muhunthan 2009, Consoli *et al.* 2013). The variation of unconfined compressive strength with cement content for 28 days cured samples is shown in Fig. 6. The unconfined compressive strength increases with cement content, which is attributed to increase of cementitious bonding between sand particles.

Fig. 7 shows the experimental results from laboratory permeability testing of cemented sand in a triaxial setup. For a particular cement content, the coefficient of permeability reduces with increase in effective confining stress. The reduction in permeability with confining stress is significant when a pressure difference of 10 kPa is used. The coefficient of permeability reduced by 85% from 50kPa to 150 kPa under a pressure difference of 10 kPa for 3% cemented sand and 69% for 5% cemented sand under similar conditions.

This sharp reduction in the coefficient of permeability was not expected because the effective confining stress used in this study is probably much less than the stress required to yield cemented sand (Cuccovillo and Coop 1997). Yielding stress, in case of cemented soils, is the minimum isotropic confining stress which induces rupture of the cemented bonds between the particles (Rotta *et al.* 2003). Before yielding, the change in void ratio of cemented soils is negligible, therefore significant reduction in coefficient of permeability may not be fully comprehended. This is confirmed by the low value of volumetric strain observed during isotropic compression of the sample (between 0.1-0.5%). This is the reason for partial reduction in permeability value observed with increase in confining pressure. Interestingly, the observed trend indicates that the use of smaller pressure difference to measure the coefficient of permeability of cemented sand might lead to inconsistent results. Similar observation was made by Carpenter and Stephenson (1986) for samples with 36 mm diameter.

Regardless of the cement content, permeability reduces with increase in hydraulic gradient. As discussed earlier, the high effective stress at the effluent end and piping could cause inaccuracy in measurement of the coefficient of permeability with increasing hydraulic gradient. Prior to yielding, the change in void ratio with increase in effective confining stress is very small (Rotta *et al.* 2003, Xiao *et al.* 2014). Hence, the use of larger hydraulic gradient could have resulted in erosion of hydrated cement products. For a given confining stress, permeability values converge at higher hydraulic gradient, as observed by Carpenter and Stephenson (1986). There are several factors such as temperature, the permeant used, hydraulic gradient, and aspect ratio of specimen that affect the measurement of the coefficient of permeability of the sample in a triaxial setup. The use of a non-destructive technique such as X-ray CT helps in understanding the hydraulic conductivity of

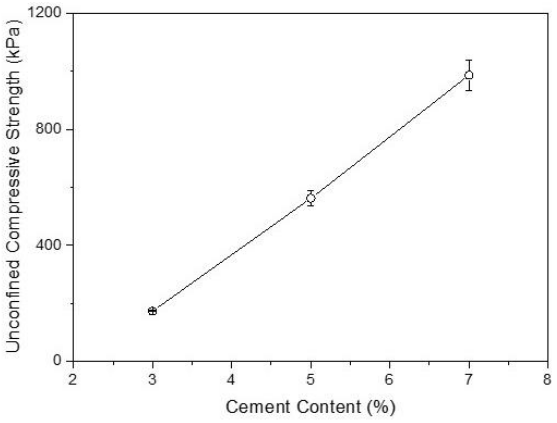

Fig. 6 Variation of unconfined compressive strength with cement content for 28 days cured samples

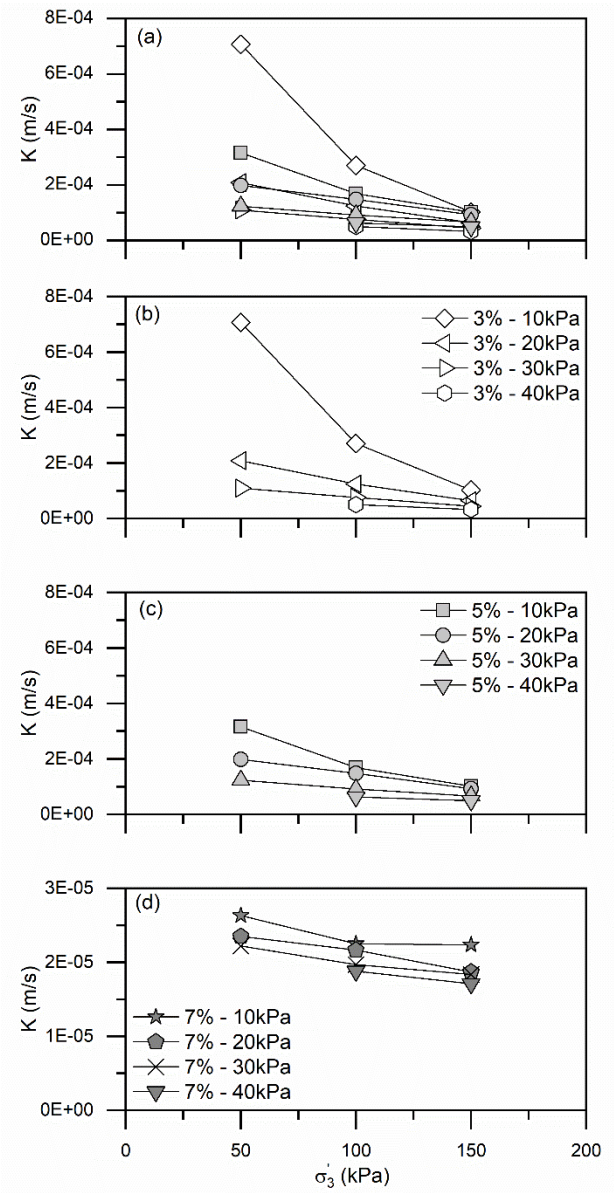

Fig. 7 Variation of permeability with effective confining stress (σ'_3) for (a) all data, (b) 3% cement content, (c) 5% cement content and (d) 7% cement content. Note – Legends also indicate applied pressure differences (10, 20, 30, 40 kPa)

cemented sand along with providing insight to the arrangement of voids inside the sample as well.

4.2 Numerical analysis for coefficient of permeability

Coefficient of permeability along the vertical axis of the sample is calculated with input pressure of 130 kPa and atmospheric pressure (1 atm) at the output end. For reference, unfortunately, we were not able to conduct laboratory testing of 1% cemented sand since the sample was heavily disturbed during extraction due to insufficient strength. However, it was possible to obtain the permeability of 1% cemented sand from image processing simulation, as X-ray CT technique obtains the microstructure of the sample without any disturbance (samples are scanned without extracting out of the mould). Fig. 8 shows variation of coefficient of permeability with cement content based on the simulation. The coefficient of permeability reduces with increase in cement content. Interestingly, it is observed that adding small amount of cement (e.g., even 1%) can lead to a significant reduction in coefficient of permeability although the trend seems quickly stabilized by adding more cement. In addition to cement content, water to cement ratio is also an important factor affecting the hydraulic conductivity of cemented sand. The amount of water present in sand affects the porosity due to random arrangement of hydrated cement products (Cardoso 2016, 2017). As the water content remains constant, the water to cement ratio of the samples reduces with increasing cement content, resulting in reduced porosity for higher cement content, thus reducing the permeability even further (Cardoso 2016). The coefficient of permeability of 3% and 5% cemented sand is almost equivalent despite the increase in unconfined compressive strength. Table 1 shows the summary of laboratory and simulation results.

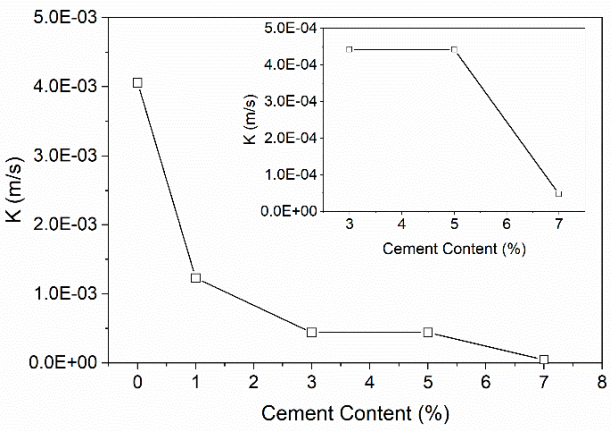

Fig. 8 Variation of permeability with cement content based on simulation results

Table 1 Mix design and summary of results

S (g)	C (g)	W (g)	w/c ratio	Mean UCS (kPa)	K lab (m/s)	K simulation (m/s)
1000	0	100	-	-	-	4.06e-3
1000	10	101	10.1	-	-	1.23e-3
1000	30	103	3.43	173	1.10e-4	4.42e-4
1000	50	105	2.10	562	1.24e-4	4.42e-4
1000	70	107	1.53	986	2.22e-5	4.74e-5

Note: S=Sand, C=Cement, W=Water, w/c=water to cement ratio

Empirical equations from Hazen (1911) and Kozeny – Carmen Bear (1972) help to predict the coefficient of permeability of geomaterials (Schwartz and Zhang 2003, Chapuis 2004). The d_{10} of the sand is 0.45 mm and the pure sand at 10% water content had a void ratio of 0.72. Thus, the coefficient of permeability computed using Hazen (1911) and Kozeny – Carmen Bear (1972) are 0.003 m/s and 0.0027 m/s. The coefficient of permeability from numerical analysis of pure sand is 0.0041 m/s, which agrees reasonably well with the empirical equations.

Fig. 9 shows the velocity field of the cemented sand samples used in this study. Velocity field helps in visualizing the flow of water through the interconnected voids in the samples. The streamlines are numerous for pure sand and decrease in number with increase in cementation, indicating the reduction in permeability of the samples.

4.3 Porosity and pore connectivity

The primary advantage of numerical analysis from the images obtained from X-ray CT is that the streamlines can be visualized, and the porosity of the samples can be

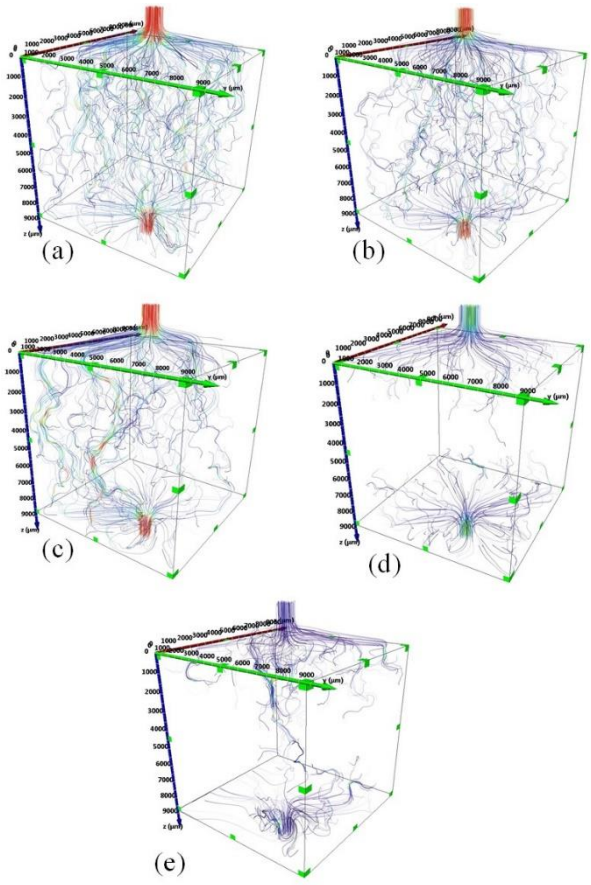

Fig. 9 Velocity field for cemented sand samples with (a) 0%, (b) 1%, (c) 3%, (d) 5% and (e) 7% cement content

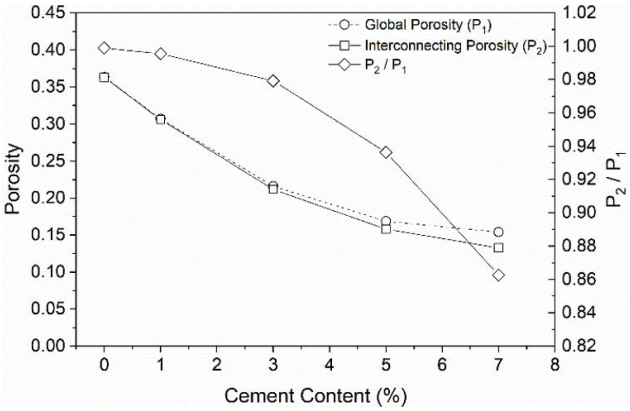

Fig. 10 Variation of porosity with cement content

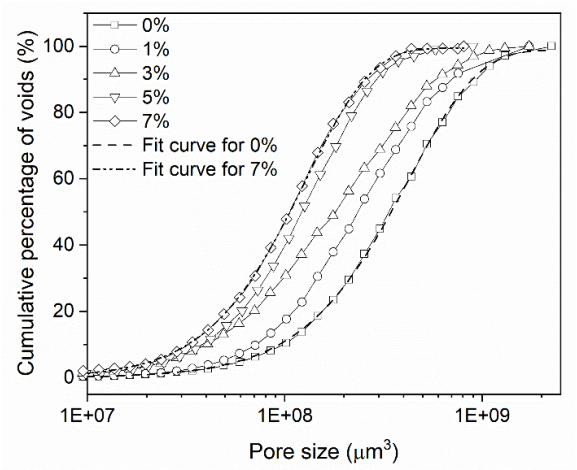

Fig. 11 Variation of cumulative percentage of voids with pore size

calculated with accuracy. The global porosity (P1) is the percentage volume of voids in the total volume of sample, while interconnecting porosity (P2) is the percentage volume of interconnected voids in the total volume of the sample. Pore size is one of the important factors affecting the permeability of the soil. From the simulation results, Fig. 10 shows the reduction in global porosity and interconnecting porosity with cement content. It was discussed earlier that the coefficient of permeability of the cemented sand reduced with cement content due to the reduction in porosity of the samples. Thus, considering the result from experimental data (Fig. 7), theoretically the porosity of 3% and 5% cemented samples should be almost equivalent.

The inter-connected porosity ratio, i.e., ratio between interconnecting porosity and global porosity, shows the proportion of interconnected voids within the total voids present in the sample. From Fig. 10 it can be seen that with increase in cement content the pore connectivity, characterized by the inter-connected porosity ratio, reduces within the samples. In an untreated sand sample, almost 100% of the voids are interconnected while in a 7% cemented sand only 86.3% of the voids are interconnected. It should be noted that these information about the interconnecting porosity and global porosity can help engineers better understand the actual seepage problems of particulate media.

Fig. 11 shows the variation of cumulative percentage voids with the pore size of the sample. The pore size indicates the volume of each pores present inside the cemented sample. The conventional void ratio and porosity represent only the overall volume of voids and does not give information about the volume of each void in the sample.

The pore size varies from 10^5 μm^3 to 2×10^9 μm^3 in the range of cement content considered in this study, but, the percentage of larger voids reduces with increase in cement content. It is well established that the increase in cement content causes a reduction in overall pore volume. In addition to containing lesser pore volume, the samples with higher cement content have more number of smaller sized voids than the lower cement content samples as shown in Fig. 12, and the presence of these small pores reduces the interconnecting voids within the sample.

Previous researchers have studied the reduction in void ratio qualitatively, while this study quantifies the actual variation in void ratio with cement content. X-Ray CT provides good insight to the microscopic pore distribution of cemented sand. Gamma cumulative distribution function (gamma CDF) is used to predict the percentage of voids less than a given pore volume. In laboratory testing, the global void ratio could be computed from phase relationship for cemented soil, then, the proposed gamma CDF could be used to compute the contribution of a given pore volume in the total volume of voids.

The gamma CDF is defined as

$$y = A_1 \times gammaCDF(x, a, b) \quad (3)$$

where A_1, a and b are offset, shape and scale parameter. The shape parameter controls the shape of the distribution, while the scale parameter defines the spread of the distribution. The offset parameter controls the magnitude of y-axis, in this study it is defined to express the y-axis in percentage. In Fig. 11, the fitting is carried out for the upper and lower boundary (0% and 7% cement content) of the cement content considered in the study. Eq. (4) is obtained for pure sand, while Eq. (5) is for 7% cemented sand.

$$y = 99 \times gammaCDF(x, 1.66, 2.55 \times 10^8) \quad (4)$$

$$y = 99 \times gammaCDF(x, 1.90, 6.69 \times 10^7) \quad (5)$$

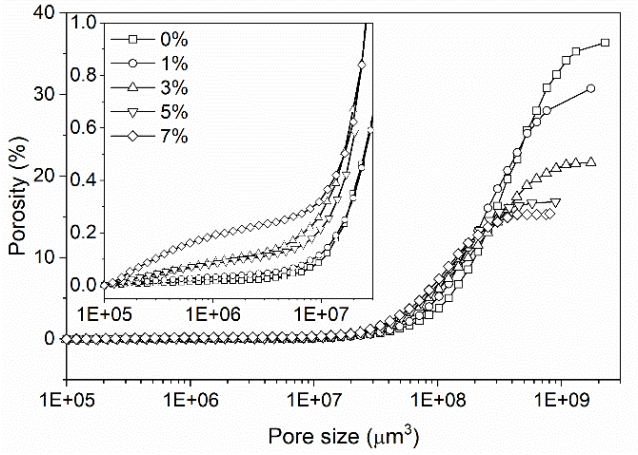

Fig. 12 Variation of porosity with pore size

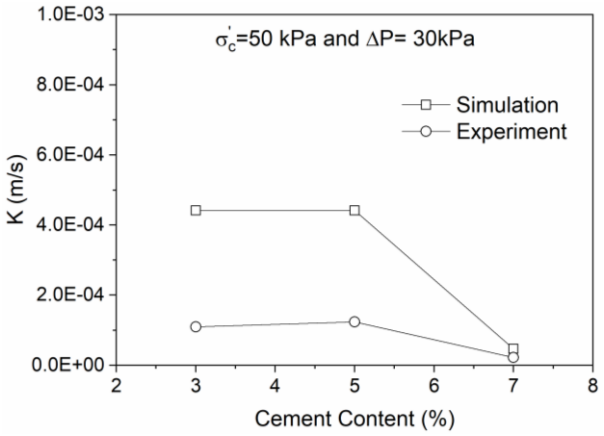

Fig. 13 Comparison of simulation and laboratory results

4.3 Comparison of coefficient of permeability – Laboratory and numerical analysis

Laboratory testing conditions involve applying a confining stress, while the difference in back pressures between top and bottom allows the water to flow through the specimen. In case of numerical analysis, the four vertical faces of the samples are closed hermetically, without any confining stress, with pressure difference (30 kPa) between two opposite faces (lateral faces) causing flow within the specimen. Hence, the coefficient of permeability under 50 kPa effective confining stress (least confining stress used in the study) and 30 kPa back pressure difference is compared against the results from numerical analysis. Fig. 13 compares the results from laboratory testing and numerical analysis.

The laboratory testing shows lower permeability values than those obtained from numerical analysis. Both numerical analysis and laboratory testing capture almost constant permeability values for 3% and 5% cement content. However, the results from numerical analysis for 3% and 5% cement content are about 3-4 times higher than the laboratory testing. The coefficient of permeability is affected by confining stress more at lower cement content. So, the difference of applied confining stress between experimental data and numerical analysis would be one of reasons for lower permeability value observed in laboratory testing. But unlike the lower cement content, laboratory and simulation results for 7% cement content samples match closer because the effect of confining stress is not significant, as observed in Fig. 7. The differences could also have been caused by differences in boundary conditions between experiment and simulation, the smaller size of the images used for simulation, and round off errors due to precision of the computer. Nevertheless, at higher cement content (7% cement content), a good agreement is observed between the simulation and experimental data.

5. Conclusions

In this study, the use of X-ray CT to analyze the microstructure and hydraulic conductivity of cemented sand was studied. The coefficients of permeability obtained from image analysis were compared with the laboratory permeability results. The effects of confining stress, hydraulic gradient and cement content on the coefficient of permeability of cemented sand were also investigated in laboratory testing. Following conclusions are drawn from this study:

• In laboratory testing, the coefficient of permeability decreases with increase in hydraulic gradient. Also, the coefficient of permeability decreases with increase in confining stress, but the use of lower hydraulic gradient resulted in erroneous results.

• The global porosity of the samples reduced with cement content, and the interconnecting voids within the total voids also reduced with cement content. These effects are reflected in both permeability and unconfined compressive strength of cemented sand samples.

• The reduction in porosity with increasing cement content results in decreasing permeability. In addition to decreasing the overall pore volume in the sample, cementation decreases the size of pores which would further reduce the permeability.

• Image processing gives a great insight to the microstructure of the cemented sand. But, the permeability results from numerical analysis on the images obtained were higher than those of laboratory testing at low cement content (e.g., 3 and 5 %). This could be due to confining stress applied during the laboratory testing. Comparable results were obtained for 7 % cement content because the effect of confining stress becomes less significant. Higher resolution of images from X-Ray CT may result in better detection of small pores in the sample, which can further improve the accuracy in segmentation process. In practice, despite the limitations, X-Ray CT would be an excellent tool to study the microstructure (e.g., microscopic pore distribution) as well as the hydraulic conductivity of cemented soils which would be subjected to structural alterations during laboratory testing.

Acknowledgments

This research was supported by the Singapore Ministry of Education (MOE).

References

Acar, Y.B. and El-Tahir, E.T.A. (1986), "Low strain dynamic properties of artificially cemented sand", *J. Geotech. Eng.*, **112**(11), 1001-1015. https://doi.org/10.1061/(ASCE)0733-9410(1986)112:11(1001).

Ajorloo, A.M., Mroueh, H. and Lancelot, L. (2012), "Experimental investigation of cement treated sand behavior under triaxial test", *Geotech. Geol. Eng.*, **30**(1), 129-143. https://doi.org/10.1061/(ASCE)0733-9410(1986)112:11(1001).

Al Qabany, A. and Soga, K. (2013), "Effect of chemical treatment used in MICP on engineering properties of cemented soils", *Géotechnique*, **63**(4), 331. https://doi.org/10.1680/bcmpge.60531.010.

Cardoso, R. (2016), "Porosity and tortuosity influence on geophysical properties of an artificially cemented sand", *Eng. Geol.*, **211**, 198-207.

https://doi.org/10.1016/j.enggeo.2016.07.009.
Cardoso, R. (2017), "Influence of water-cement ratio on the hydraulic behavior of an artificially cemented sand", *Geotech. Geol. Eng.*, **35**(4), 1513-1527. https://doi.org/10.1007/s10706-017-0190-3.
Carpenter, G. and Stephenson, R. (1986), "Permeability testing in the triaxial cell", *Geotech. Test. J.*, **9**(1), 3-9. https://doi.org/10.1520/GTJ10605J.
Chapuis, R.P. (2004), "Predicting the saturated hydraulic conductivity of sand and gravel using effective diameter and void ratio", *Can. Geotech. J.*, **41**(5), 787-795. https://doi.org/10.1139/t04-022.
Chen, B., Sun, D. and Jin, P. (2019), "Experimental study of the effect of microstructure on the permeability of saturated soft clays", *Geomech. Eng.*, **18**(1), 49-58. https://doi.org/10.12989/gae.2019.18.1.049.
Choi, S.G., Chu, J. and Kwon, T.H. (2019), "Effect of chemical concentrations on strength and crystal size of biocemented sand", *Geomech. Eng.*, **17**(5), 465-473. https://doi.org/10.12989/gae.2019.17.5.465.
Clough, G.W., Sitar, N., Bachus, R.C. and Rad, N.S. (1981), "Cemented sands under static loading", *J. Geotech. Geoenviron. Eng.*, **107**(6), 799-817.
Consoli, N.C., Cruz, R.C., Floss, M.F. and Festugato, L. (2009), "Parameters controlling tensile and compressive strength of artificially cemented sand", *J. Geotech. Geoenviron. Eng.*, **136**(5), 759-763. https://doi.org/10.1061/(ASCE)GT.1943-5606.0000278.
Consoli, N.C., Festugato, L., da Rocha, C.G. and Cruz, R.C. (2013), "Key parameters for strength control of rammed sand–cement mixtures: Influence of types of portland cement", *Construct. Build. Mater.*, **49**, 591-597. https://doi.org/10.1016/j.conbuildmat.2013.08.062.
Consoli, N.C., Foppa, D., Festugato, L., and Heineck, K.S. (2007), "Key parameters for strength control of artificially cemented soils", *J. Geotech. Geoenviron. Eng.*, **133**(2), 197-205. https://doi.org/10.1061/(ASCE)1090-0241(2007)133:2(197).
Crestana, S., Mascarenhas, S. and Pozzi-Mucelli, R.S. (1985), "Static and dynamic three dimensional studies of water in soil using computed tomographic scanning", *Soil Sci.*, **140**(5), 326-332.
Cuccovillo, T. and Coop, M. (1997), "Yielding and pre-failure deformation of structured sands", *Géotechnique*, **47**(3), 491-508. https://doi.org/10.1680/geot.1997.47.3.491.
Daniel, D.E. (1994), *State-of-the-Art: Laboratory Hydraulic Conductivity Tests for Saturated Soils*, in *Hydraulic Conductivity and Waste Contaminant Transport in Soil*, ASTM International.
DeJong, J.T., Fritzges, M.B. and Nüsslein, K. (2006), "Microbially induced cementation to control sand response to undrained shear", *J. Geotech. Geoenviron. Eng.*, **132**(11), 1381-1392. https://doi.org/10.1061/(ASCE)1090-0241(2006)132:11(1381).
DeJong, J.T., Mortensen, B.M., Martinez, B.C. and Nelson, D.C. (2010), "Bio-mediated soil improvement", *Ecol. Eng.*, **36**(2), 197-210. https://doi.org/10.1016/j.ecoleng.2008.12.029.
Dunn, R.J. and Mitchell, J.K. (1984), "Fluid conductivity testing of fine-grained soils", *J. Geotech. Eng.*, **110**(11), 1648-1665. https://doi.org/10.1061/(ASCE)0733-9410(1984)110:11(1648).
Edil, T.B. and Erickson, A.E. (1985), *Procedure and Equipment Factors affecting Permeability Testing of a Bentonite-Sand Liner Material*, in *Hydraulic Barriers in Soil and Rock*, ASTM International.
Fernandez, A.L. and Santamarina, J.C. (2001), "Effect of cementation on the small-strain parameters of sands", *Can. Geotech. J.*, **38**(1), 191-199. https://doi.org/10.1139/t00-081.
Ferris, F.G., Stehmeier, L.G., Kantzas, A. and Mourits, F.M. (1996), "Bacteriogenic mineral plugging", *J. Can. Petrol. Technol.*, **35**(08). https://doi.org/10.2118/97-09-07.
Fox, P.J. (1996), "Analysis of hydraulic gradient effects for laboratory hydraulic conductivity testing", *Geotech. Test. J.*, **19**(2), 181-190. https://doi.org/10.1520/GTJ10340J.
Garboczi, E.J. and Bentz, D.P. (2001), "The effect of statistical fluctuation, finite size error, and digital resolution on the phase percolation and transport properties of the NIST cement hydration model", *Cement Concrete Res.*, **31**(10), 1501-1514. https://doi.org/10.1016/S0008-8846(01)00593-2.
Hainsworth, J.M. and Aylmore, L.A.G. (1983), "The use of computer assisted tomography to determine spatial distribution of soil water content", *Soil Res.*, **21**(4), 435-443. https://doi.org/10.1071/SR9830435.
Hang, L., Gao, Y., He, J. and Chu, J. (2019), "Mechanical behaviour of biocemented sand under triaxial consolidated undrained or constant shear drained conditions", *Geomech. Eng.*, **17**(5), 497-505. https://doi.org/10.12989/gae.2019.17.5.497.
Heeraman, D.A., Hopmans, J.W. and Clausnitzer, V. (1997), "Three dimensional imaging of plant roots in situ with X-ray computed tomography", *Plant Soil*, **189**(2), 167-179. https://doi.org/10.1023/B:PLSO.0000009694.64377.6f.
Kawaragi, C., Yoneda, T., Sato, T. and Kaneko, K. (2009), "Microstructure of saturated bentonites characterized by X-ray CT observations", *Eng. Geol.*, **106**(1), 51-57. https://doi.org/10.1016/j.enggeo.2009.02.013.
Ketcham, R.A. and Carlson, W.D. (2001), "Acquisition, optimization and interpretation of X-ray computed tomographic imagery: Applications to the geosciences", *Comput. Geosci.*, **27**(4), 381-400. https://doi.org/10.1016/S0098-3004(00)00116-3.
Khan, Q., Subramanian, S., Wong, D.Y.C. and Ku, T. (2019), "Bender elements in stiff cemented clay: Shear wave velocity correction by applying wavelength considerations", *Can. Geotech. J.*, **56**(7), 1034-1041. https://doi.org/10.1139/cgj-2018-0153.
Kozaki, T., Suzuki, S., Kozai, N., Sato, S. and Ohashi, H. (2001), "Observation of microstructures of compacted bentonite by microfocus X-ray computerized tomography (Micro-CT)", *J. Nucl. Sci. Technol.*, **38**(8), 697-699. https://doi.org/10.1080/18811248.2001.9715085.
Ladd, R.S. (1978), "Preparing test specimens using under compaction", *Geotech. Test. J.*, **1**(1), 16-23. https://doi.org/10.1520/GTJ10364J.
Lee, C., Nam, H., Lee, W., Choo, H. and Ku, T. (2019), "Estimating UCS of cement-grouted sand using characteristics of sand and UCS of pure grout", *Geomech. Eng.*, **19**(4), 343-352. https://doi.org/10.12989/gae.2019.19.4.343.
Leonards, G.A., Huang, A.B. and Ramos, J. (1991), "Piping and erosion tests at Conner Run Dam", *J. Geotech. Eng.*, **117**(1), 108-117. https://doi.org/10.1061/(ASCE)0733-9410(1991)117:1(108).
Moon, S.W., Vinoth, G., Subramanian, S., Kim, J. and Ku, T. (2019), "Effect of fine particles on strength and stiffness of cement treated sand", *Granul. Matter*, **22**, 9. https://doi.org/10.1007/s10035-019-0975-6.
Mooney, S.J. (2002), "Three dimensional visualization and quantification of soil macroporosity and water flow patterns using computed tomography", *Soil Use Manage.*, **18**(2), 142-151. https://doi.org/10.1111/j.1475-2743.2002.tb00232.x.
Narsilio, G.A., Buzzi, O., Fityus, S., Yun, T.S. and Smith, D.W. (2009), "Upscaling of Navier-Stokes equations in porous media: Theoretical, numerical and experimental approach", *Comput. Geotech.*, **36**(7), 1200-1206. https://doi.org/10.1016/j.compgeo.2009.05.006.
Nunan, N., Ritz, K., Rivers, M., Feeney, D.S. and Young, I.M. (2006), "Investigating microbial micro-habitat structure using

X-ray computed tomography", *Geoderma*, **133**(3), 398-407. https://doi.org/10.1016/j.geoderma.2005.08.004.

Olson, R.E. and Daniel, D.E. (1981), *Measurement of the Hydraulic Conductivity of Fine-Grained Soils*, in *Permeability and Groundwater Contaminant Transport*, ASTM International.

Park, D., Kim, I., Kim, G. and Lee, J. (2019), "Effect of groundwater fluctuation on load carrying performance of shallow foundation", *Geomech. Eng.*, **18**(6), 575-584. https://doi.org/10.12989/gae.2019.18.6.575.

Peng, S., Marone, F. and Dultz, S. (2014), "Resolution effect in X-ray microcomputed tomography imaging and small pore's contribution to permeability for a Berea sandstone", *J. Hydrol.*, **510**, 403-411. https://doi.org/10.1016/j.jhydrol.2013.12.028.

Petrovic, A.M., Siebert, J.E. and Rieke, P.E. (1982), "Soil bulk density analysis in three dimensions by computed tomographic scanning", *Soil Sci. Soc. Amer. J.*, **46**(3), 445-450. https://doi.org/10.2136/sssaj1982.03615995004600030001x.

Pierret, A., Capowiez, Y., Belzunces, L. and Moran, C.J. (2002), "3D reconstruction and quantification of macropores using X-ray computed tomography and image analysis", *Geoderma*, **106**(3), 247-271. https://doi.org/10.1016/S0016-7061(01)00127-6.

Provis, J.L., Myers, R.J., White, C.E., Rose, V. and van Deventer, J.S.J. (2012), "X-ray microtomography shows pore structure and tortuosity in alkali-activated binders", *Cement Concrete Res.*, **42**(6), 855-864.

Rogasik, H., Onasch, I., Brunotte, J., Jegou, D. and Wendroth, O. (2003), "Assessment of soil structure using X-ray computed tomography", *Geol. Soc. London Special Publ.*, **215**(1), 151-165. https://doi.org/10.1144/GSL.SP.2003.215.01.14.

Rotta, G.V., Consoli, N.C., Prietto, P.D.M., Coop, M.R. and Graham, J. (2003), "Isotropic yielding in an artificially cemented soil cured under stress", *Geotechnique*, **53**(5), 493-501. https://doi.org/10.1680/geot.2003.53.5.493.

Sariosseiri, F. and Muhunthan, B. (2009), "Effect of cement treatment on geotechnical properties of some Washington State soils", *Eng. Geol.*, **104**(1), 119-125. https://doi.org/10.1016/j.enggeo.2008.09.003.

Sarkar, G. and Siddiqua, S. (2016), "Effect of fluid chemistry on the microstructure of light backfill: An X-ray CT investigation", *Eng. Geol.*, **202**, 153-162. https://doi.org/10.1016/j.enggeo.2016.01.012.

Saxena, S.K., Avramidis, A.S. and Reddy, K.R. (1988), "Dynamic moduli and damping ratios for cemented sands at low strains", *Can. Geotech. J.*, **25**(2), 353-368. https://doi.org/10.1139/t88-036.

Schnaid, F., Prietto, P.D.M. and Consoli, N.C. (2001), "Characterization of cemented sand in triaxial compression", *J. Geotech. Geoenviron. Eng.*, **127**(10), 857-868. https://doi.org/10.1061/(ASCE)1090-0241(2001)127:10(857).

Schwartz, F.W. and Zhang, H. (2003), *Fundamentals of Groundwater*, John Wiley & Sons. New York, U.S.A.

Sidik, W.S., Canakci, H., Kilic, I.H. and Celik, F. (2014), "Applicability of biocementation for organic soil and its effect on permeability", *Geomech. Eng.*, **7**(6), 649-663. https://doi.org/10.12989/gae.2014.7.6.649.

Subramanian, S., Khan, Q. and Ku, T. (2019), "Strength development and prediction of calcium sulfoaluminate treated sand with optimized gypsum for replacing OPC in ground improvement", *Construct. Build. Mater.*, **202**, 308-318. https://doi.org/10.1016/j.conbuildmat.2018.12.121.

Subramanian, S., Moon, S.W., Moon, J. and Ku, T. (2018), "CSA treated sand for ground improvement: Microstructure analysis and rapid strength development", *J. Mater. Civ. Eng.*, **30**(12), 04018313. https://doi.org/10.1061/(ASCE)MT.1943-5533.0002523.

Uchikawa, H. (1989), "Similarities and discrepancies of hardened cement paste, mortar and concrete from the standpoints of composition and structure", *Proceeding of the Engineering Foundation Conference' Advances in Cement Manufacture and Use'at Trout Lodge*, Potosi, Missouri, U.S.A.

Viggiani, G., Andò, E., Takano, D. and Santamarina, J.C. (2015), "Laboratory X-ray tomography: A valuable experimental tool for revealing processes in soils", *Geotech. Test. J.*, **38**(1), 61-70. https://doi.org/10.1520/GTJ20140060.

Wang, Y.H. and Leung, S.C. (2008), "A particulate-scale investigation of cemented sand behavior", *Can. Geotech. J.*, **45**(1), 29-44. https://doi.org/10.1139/T07-070.

Wei, X. and Ku, T. (2020), "New design chart for geotechnical ground improvement: Characterizing cement-stabilized sand", *Acta Geotechnica*, **15**(4), 999-1011. https://doi.org/10.1007/s11440-019-00838-2.

Xiao, H., Lee, F.H. and Chin, K.G. (2014), "Yielding of cement-treated marine clay", *Soils Found.*, **54**(3), 488-501. https://doi.org/10.1016/j.sandf.2014.04.021.

Yilmaz, Y., Eun, J. and Goren, A. (2018), "Individual and combined effect of Portland cement and chemical agents on unconfined compressive strength for high plasticity clayey soils", *Geomech. Eng.*, **16**(4), 375-384. https://doi.org/10.12989/gae.2018.16.4.375.

Young, I.M., Crawford, J.W. and Rappoldt, C. (2001), "New methods and models for characterising structural heterogeneity of soil", *Soil Tillage Res.*, **61**(1), 33-45. https://doi.org/10.1016/S0167-1987(01)00188-X.

IC